

Better Optimization of Variational Quantum Eigensolvers by combining the Unitary Block Optimization Scheme with Classical Post-Processing

Xiaochuan Ding* and Bryan K. Clark†

Physics Department, University of Illinois at Urbana-Champaign

(Dated: May 13, 2024)

Variational Quantum Eigensolvers (VQE) are a promising approach for finding the classically intractable ground state of a Hamiltonian. The Unitary Block Optimization Scheme (UBOS) is a state-of-the-art VQE method which works by sweeping over gates and finding optimal parameters for each gate in the environment of other gates. UBOS improves the convergence time to the ground state by an order of magnitude over Stochastic Gradient Descent (SGD). It nonetheless suffers in both rate of convergence and final converged energies in the face of highly noisy expectation values coming from shot noise. Here we develop two classical post-processing techniques which improve UBOS especially when measurements have large noise. Using Gaussian Process Regression (GPR), we generate artificial augmented data using original data from the quantum computer to reduce the overall error when solving for the improved parameters. Using Double Robust Optimization plus Rejection (DROPR), we prevent outlying data which are atypically noisy from resulting in a particularly erroneous single optimization step thereby increasing robustness against noisy measurements. Combining these techniques further reduces the final relative error that UBOS reaches by a factor of three without adding additional quantum measurement or sampling overhead. This work further demonstrates that developing techniques which use classical resources to post-process quantum measurement results can significantly improve VQE algorithms.

I. INTRODUCTION

In the near term, quantum computers are limited by qubit coherence and gate fidelity. These early noisy intermediate-scale quantum (NISQ) devices [1] have too few physical qubits with high coherence time to implement robust error correction schemes, making them unsuitable for many promising quantum algorithms such as Shor’s algorithm [2–9] and Grover’s algorithm [10–15]. To avoid these issues, hybrid classical-quantum algorithms like the quantum approximate optimization algorithm (QAOA) [16] and the variational quantum eigensolver (VQE) [17–19] leverage the resources of a quantum computer to simulate and sample from a classically intractable state while using classical resources to reduce the demand on qubits and coherence.

VQE aims to compute an upper bound for the ground-state energy of a Hamiltonian \hat{H} , which is generally the first step in computing the properties of molecules and materials [20–23]. Starting with an *ansatz* which is a quantum circuit built with a set of parametrized quantum gates to model a trial wavefunction, $|\Psi\rangle$, VQE iteratively optimizes the gate parameters of the *ansatz* to minimize the energy of the trial state by computing the expectation values of operators in the Hamiltonian through measurements on the quantum computer; and then classically updating the gate parameters.

Given the stochastic nature of measurement on quantum devices [24], one must measure enough copies (denoted as shots) of the same circuit to achieve a given level

of precision since the distribution of measurement outcomes has error inversely proportional to square root of the number of shots per circuit. The standard approach to VQE has been improved in various ways including *ansatz* construction [17, 25–31], efficient measurement strategy [32–42], error mitigation techniques [43–56], and optimization strategies [57–67]. Classical machine learning techniques such as Koopman Operator Learning [68] and physics-informed neural network [69] have also been used to improve VQE.

Typical optimization strategies for VQE algorithms are gradient-free classical optimization methods including Nelder-Mead method and Powell’s algorithm [64, 65, 70], gradient-based searching strategy [25, 31, 63, 71–82], and analytical methods such as Anderson Acceleration [66]. Traditional methods such as Stochastic Gradient Descent (SGD) face several challenges including local minima, significant hyperparameter tuning, slow convergence, and exponentially vanishing gradients.

The unitary block optimization scheme (UBOS) is a gradient-free and hyperparameter-free optimization algorithm [83]. By optimizing a subset of parameters at each step using the effective Hamiltonian \tilde{H} , it avoids gradient calculation, tunnels through some local minima, makes nontrivial steps decreasing the energy when facing barren plateaus, and requires an order of magnitude less expectation value measurements than Stochastic Gradient Descent (SGD).

The key step of UBOS is to generate the effective Hamiltonian for a gate in a fixed environment. The standard approach to accomplish this is to directly measure the matrix elements using a separate quantum circuit for each element; this approach we refer to as *D-UBOS*. An alternative approach is to infer the effective Hamiltonian from pairs of gate parameters and their corresponding

* xd13@illinois.edu

† bkclark@illinois.edu

energies $\{(t_j, E_{measured})\}$, which we will refer to as **E-UBOS**.

One of the primary concerns for VQE algorithms is its shot budget (total amount of measurements). One approach to reducing the shot budget is to simply take fewer measurements per circuit resulting in much larger stochastic errors due to the finite number of shots (denoted as shot noise). Significant shot noise often hinders classical optimizers from finding the true global minimum; many methods including UBOS plateau at an energy level above the optimal VQE energy of the ansatz (VQEOPT). This raises scalability concerns for the VQE algorithm [84–86].

For UBOS, noise in quantum measurements causes error in the effective Hamiltonian \tilde{H} which leads to inaccurate state energy estimation using \tilde{H} . D-UBOS has no measure against such noise. In E-UBOS one can partially mitigate noise by increasing the number of $(t_j, E_{measured})$ pairs at the cost of additional quantum measurements. Unfortunately, when we empirically compare, E-UBOS as naively formulated still requires the same amount or slightly more shot budget to reach the same energy error as D-UBOS (see Fig. 3).

In this paper, we develop generalizations of E-UBOS to resolve this problem. Our philosophy is that while the classical optimization of the gate parameters for the exact effective Hamiltonian is straightforward, classical noise-aware post-processing techniques can help reach a better energy without taxing the shot budget, especially when the quantum measurements are very noisy. We introduce two techniques: Data Augmentation with Gaussian Process Regression (GPR) and Double Robust Optimization plus Rejection (DROPR). We demonstrate that these two classical post-processing techniques can effectively suppress the noise in quantum measurements and reduce the relative energy error of the full optimization roughly by a factor of 3 for all choices of hyperparameters in the range studied.

The rest of the paper is organized as follows: In Sec. II we briefly review how to implement different types of UBOS. Next, in Sec. III, we describe the classical post-processing techniques. Then in Sec. IV we benchmark the performance of E-UBOS with these techniques applied and compare it with D-UBOS. Finally, we conclude the paper in Sec. V with a discussion of our main results.

II. INTRODUCTION TO UBOS METHODS

A. Review of UBOS

In this paper we describe all types of UBOS using a variational ansatz,

$$|\psi\rangle = \prod_{j=1}^K U_j |0\rangle \quad (1)$$

obtained by applying K generic two-qubit unitaries $U_j \in SU(4)$ (i.e., quantum gates), to adjacent qubits in a brickwork pattern with gate depth d . The generic two-qubit unitary, U_j , can be written as a linear combination of 16 two-qubit Pauli strings,

$$U_j = \sum_{\alpha, \beta=0}^3 t_j^{\alpha\beta} P^{\alpha\beta} \quad (2)$$

where $P^{\alpha\beta} = \sigma^\alpha \sigma^\beta$, $\sigma^{\alpha, \beta} \in \{I, X, Y, Z\}$ are Pauli matrices, and the complex coefficient $t_j^{\alpha\beta}$ are constrained to preserve the unitarity of U_j (see Appendix A).

UBOS then parameterizes the state by the gate parameters $\{t_1, t_2 \dots t_K\}$ where $t_j \equiv (t_j^{00}, t_j^{01} \dots t_j^{33})$,

$$\begin{aligned} |\psi\rangle &= \left(\prod_{k=1}^{j-1} U_k \right) U_j \left(\prod_{k=j+1}^K U_k \right) |0\rangle \\ &= \left(\prod_{k=1}^{j-1} U_k \right) \left(\sum_{\alpha, \beta=0}^3 t_j^{\alpha\beta} P^{\alpha\beta} \right) \left(\prod_{k=j+1}^K U_k \right) |0\rangle \\ &= \sum_{\alpha, \beta=0}^3 t_j^{\alpha\beta} \left| \psi_j^{\alpha\beta} \right\rangle \end{aligned} \quad (3)$$

where

$$\left| \psi_j^{\alpha\beta} \right\rangle = \left(\prod_{k=1}^{j-1} U_k \right) P^{\alpha\beta} \left(\prod_{k=j+1}^K U_k \right) |0\rangle \quad (4)$$

is the result of substituting gate U_j by the Pauli operator $P^{\alpha\beta}$ and has the same circuit depth d . It is also the derivative of $|\psi\rangle$ with respect to $t_j^{\alpha\beta}$

Given some Hamiltonian \hat{H} , keeping the parameters for all but the j th gate fixed, UBOS writes the energy as a function of the j th gate parameters,

$$\begin{aligned} E(\mathbf{t}_j) &= \langle \psi | \hat{H} | \psi \rangle \\ &= \left(\sum_{\alpha', \beta'=0}^3 t_j^{*\alpha' \beta'} \left\langle \psi_j^{\alpha' \beta'} \right| \right) \hat{H} \left(\sum_{\alpha, \beta=0}^3 t_j^{\alpha\beta} \left| \psi_j^{\alpha\beta} \right\rangle \right) \\ &= \sum_{\alpha, \beta, \alpha', \beta'=0}^3 t_j^{*\alpha' \beta'} \tilde{H}^{\alpha' \beta'; \alpha\beta} t_j^{\alpha\beta} \end{aligned} \quad (5)$$

$$= \mathbf{t}_j^\dagger \tilde{H} \mathbf{t}_j \quad (6)$$

with the effective Hamiltonian for gate j , \tilde{H} as

$$\tilde{H}^{\alpha' \beta'; \alpha\beta} = \left\langle \psi_j^{\alpha' \beta'} \right| \hat{H} \left| \psi_j^{\alpha\beta} \right\rangle. \quad (7)$$

\tilde{H} is a 16×16 Hermitian matrix with 256 unique real parameters for its matrix elements (136 for real component and 120 for imaginary component), and is independent of t_j .

Once \tilde{H} is obtained, UBOS classically optimizes the gate parameters for the j th gate while keeping all other

gates fixed by minimizing Eq. 6 with respect to the gate parameters \mathbf{t}_j under the unitary constraint (see Appendix A). This is a 16-parameter optimization problem that can be solved using any classical technique such as gradient descent, Nelder-Mead, etc. UBOS then sweeps over gates, optimally minimizing the energy of one gate at a time while keeping other gates temporarily fixed. The update order for gates is shuffled to be random for every sweep, a.k.a. epoch.

To obtain the effective Hamiltonian, D-UBOS directly measures these matrix elements with Hadamard test circuits of depth at most $2d$ (see Appendix B), where the Hamiltonian is expanded into the sum of unitary operators. The expectation value measurement of each Hamiltonian component requires (many copies of) a separate circuit and the measurement accuracy depends on the hardware noise and the number of shots per circuit (denoted as n_{shots}). The total number of measurements N_{meas} scales as $O(dn_q^2 n_{shots})$ (see Appendix C) where n_q is the number of qubits and d is the ansatz depth.

B. Review of E-UBOS

As described in Appendix G of the original UBOS paper [83], the matrix elements of \tilde{H} in Eq. 6 are linear unknowns and independent of the gate parameters at the j th gate, so instead of measuring them individually, we can solve for them from a system of linear equations obtained by measuring the energies of the states with the j th gate replaced by a two-qubit unitary generated with different, randomly chosen gate parameters. One advantage of this approach is that the depth of the circuit required for measurement is only d (see Appendix B).

By writing t_j and \tilde{H} as their complex form, $t_j = \text{Re}[t_j] + i \text{Im}[t_j]$ and $\tilde{H} = \text{Re}[\tilde{H}] + i \text{Im}[\tilde{H}]$, We can rewrite Eq. 5 as

$$\begin{aligned} E(\mathbf{t}_j) &= \sum_{m,n=0}^{15} t_j^{*n} \tilde{H}^{n;m} t_j^m \\ &= \sum_{m,n=0}^{15} t_{j,R}^{nm} \text{Re}[\tilde{H}^{n;m}] - t_{j,I}^{nm} \text{Im}[\tilde{H}^{n;m}] \end{aligned} \quad (8)$$

where

$$t_{j,R}^{nm} \equiv \text{Re}[t_j^{*n} t_j^m] = \text{Re}[t_j^n] \text{Re}[t_j^m] - \text{Im}[t_j^n] \text{Im}[t_j^m] \quad (9)$$

$$t_{j,I}^{nm} \equiv \text{Im}[t_j^{*n} t_j^m] = \text{Re}[t_j^n] \text{Im}[t_j^m] + \text{Im}[t_j^n] \text{Re}[t_j^m] \quad (10)$$

are quadratic forms of the t_j components. Therefore, every random gate parameter vector t_j corresponds to a noiseless energy E .

We generate random t_j by sampling a random two-qubit unitary from the unitary Haar measure and then performing decomposition in the Pauli basis.

State energies are calculated by $E = \sum_i \text{Tr}(\rho_i \hat{h}_i)$ where \hat{h}_i are the components of the Hamiltonian

and ρ_i is the corresponding reduced density matrix. Since the Hamiltonian studied contains only local $\{Z, XX, YY, ZZ\}$ operators, by measuring their expectation values on quantum devices (see Appendix B), we obtain the measured state energy, $E_{measured}$, which is a stochastically noisy *observation* of pair $(t_j, E_{measured})$. To characterize noise in the measured energy, we can write $E_{measured}$ as

$$E_{measured} = E + \delta E = \mathbf{t}_j^\dagger \tilde{H} \mathbf{t}_j + \delta E \quad (11)$$

where δE is the error in the measured state energy.

Given n_{obs} pairs of $(t_j, E_{measured})$, we can form a system of n_{obs} linear equations and determine \tilde{H} by linear least squares fit over the system. The number of linearly independent components in the set $T_j \equiv \{t_{j,R}^{nm} \cup t_{j,I}^{nm}\}$ is found to be 226 and is smaller than 256, the number of unique real parameters in the 16×16 Hermitian matrix \tilde{H} , which leads to non-unique effective Hamiltonian that satisfies Eq. 8. However, any effective Hamiltonian that satisfies Eq. 8, or equivalently, Eq. 6, is suitable for optimization, and by increasing n_{obs} to overconstrain the system, we can add additional robustness against error in measured state energy which is normally reduced by increasing shots per circuit, n_{shots} . In other words, to increase the accuracy of the effective Hamiltonian, one can use larger n_{obs} to compensate for the large stochastic noise due to small n_{shots} and vice versa (note that the minimum value of n_{obs} is 226).

III. CLASSICAL POST-PROCESSING FOR E-UBOS

In the current applications of UBOS, the effective Hamiltonian at each step is computed from a finite number of shots which results in a noisy effective Hamiltonian which we assume to be ‘exact’ when computing the new parameters. Here we suggest an alternative approach which does a significant amount of classical post-processing on the data gained from E-UBOS (and sometimes additional quantum post-processing). This classical post-processing can be aware of the noisy nature of the measurements allowing it to better select new parameters. In this paper, we introduce two techniques: Data Augmentation with Gaussian Process Regression (GPR) and Double Robust Optimization plus Rejection (DROPR) inspired from approaches in machine learning.

A. Data Augmentation with Gaussian Process Regression

An E-UBOS optimization step involves three parts: first, it obtains a set of $(t_j, E_{measured})$ pairs through quantum measurements. For convenience, we will refer to this set as the *initial set*, denoted by S_{init} . Then, it computes the effective Hamiltonian from a system of linear equations formed with S_{init} . Finally, it classically

finds the gate parameters that minimizes the state energy based on the obtained effective Hamiltonian. When the number of shots per circuit is small, large shot noise in pairs in S_{init} can cause severe error in the calculated effective Hamiltonian.

One could increase the accuracy of the effective Hamiltonian by having more $(t_j, E_{measured})$ pairs but this would obviously involve a larger shot budget. An alternative to this approach is to generate artificial pairs using ‘‘Data Augmentation’’ [87–89] in such a way that expanding S_{init} with this additional artificial data will lead to more accurate estimation of the effective Hamiltonian. Artificial data is created by predicting the energy of new random t_j based on existing observations. Traditional algorithms such as least squares regression suffer from the large noise in each observation and the nonlinear relationship between the features (gate parameters) and the target (energy). An alternative approach is to use Gaussian Process Regression, which returns an evidence-based posterior probability distribution over possible functions that fit a set of points [90, 91]. Here we describe how GPR can be used to generate new artificial data for our VQE energies including for completeness the underlying theory for how GPR selects the new data.

We assume that the noise in the measured energy follows some Gaussian distribution, $\delta E \sim N(0, \sigma_\epsilon^2)$, such that for each random gate parameters t_j , the corresponding measured energy follows the normal distribution $E_{measured} \sim N(E, \sigma_\epsilon^2)$ where E is the noiseless energy. Then we can model the collection of measured energies as a multi-variate normal (MVN) distribution $P(\{E_{measured}\}|\{t_j\})$. Any sample from this MVN distribution would correspond to a function which is possibly suitable to describe the relationship between the various t_j and E . However these functions are very unlikely to be smooth enough for regression purpose and the number of possible functions is infinite. Therefore, we determine the possible functions by sampling with a kernel function which measures the similarity (covariance) between two t_j ’s, following the logic that similar t_j ’s should lead to similar E ’s. This constitutes our prior which is a collection of infinite numbers of smooth functions derived with the kernel and its mean function equals to zero.

We can write a collection of observed data and artificial data as $\{(t_{j,obs}, E_{measured})\}$ and $\{(t_{j,new}, E_{predict})\}$, respectively, where $E_{predict}$ ’s are unknown. Then we can model $E_{measured}$ and $E_{predict}$ as a MVN distribution in block matrix notation:

$$P(\{E_{measured}\}, \{E_{predict}\}|\{t_{j,obs}\}, \{t_{j,new}\}) \sim N\left(\begin{bmatrix} M_{obs}(\{t_{j,obs}\}) \\ M_{new}(\{t_{j,new}\}) \end{bmatrix}, \begin{bmatrix} \hat{K}_{obs,obs} & K_{obs,new} \\ K_{obs,new}^T & K_{new,new} \end{bmatrix}\right) \quad (12)$$

where M_{obs} and M_{new} are the mean functions of the MVN distribution for the collection of observed data and artificial data, respectively. $\hat{K}_{obs,obs} = K_{\{t_{j,obs}\}, \{t_{j,obs}\}} +$

σ_ϵ^2 is the covariance matrix between all t_j in the observed data with noise added. $K_{obs,new} = K_{\{t_{j,obs}\}, \{t_{j,new}\}}$ and $K_{new,new} = K_{\{t_{j,new}\}, \{t_{j,new}\}}$ are the covariance matrices between all t_j in the observed data and in the artificial data and between all t_j in the artificial data, respectively.

Now our observations $\{(t_{j,obs}, E_{measured})\}$ become partial observations of this joint normal distribution. Therefore, by Marginal and Conditional Distribution of Multivariate Normal Distribution Theorem, we can find that the conditional probability distribution of the predicted energies follows the MVN in block matrix notation

$$P(\{E_{predict}\}|\{E_{measured}\}, \{t_{j,obs}\}, \{t_{j,new}\}) \sim N(\mu, \Sigma) \quad (13)$$

where $\mu = K_{obs,new}^T \hat{K}_{obs,obs}^{-1} \{E_{measured}\}$ and $\Sigma = K_{new,new} - K_{obs,new}^T \hat{K}_{obs,obs}^{-1} K_{obs,new}$ are its mean and covariance, respectively. The mean value of each feature of this MVN is then the predicted energy for each artificial t_j with maximum likelihood.

Equivalently, one can explicitly find the probability distribution of possible functions f instead of energies. In this way, one sees that Gaussian Process uses some kernel function to generate a prior for probability distribution of possible functions and calculates the posterior probability distribution of the functions for the observed data (evidence), $P(\{f_{measured}\}|\{(t_{j,obs}, E_{measured})\})$, which is similar to Bayesian Inference process. Then, it repeats the same formalism as in Eq. 12 and Eq. 13 with energy terms replaced by corresponding function terms.

Gaussian Process Regression is more useful in this data augmentation task than least squares regression. It relaxes the form of the predicted model from one function to a probability distribution of possible functions, which is more effective in dealing with the nonlinear relationship between t_j and E and the non-unique effective Hamiltonians that fit the observations well.

We propose the following scheme of performing data augmentation using Gaussian Process Regression (GPR): we assemble overlapping subsets of $(t_j, E_{measured})$ pairs from S_{init} , train a Gaussian Process model using Gaussian Process Regressor for each subset, generate artificial $(t_j, E_{predict})$ pairs by applying those models on new random gate parameters t_j , and merge them with the S_{init} to create an expanded data set. See Appendix E for a detailed discussion of hyperparameter choices for this technique.

In the ideal GPR data augmentation scheme, subsets of pairs will not overlap with each other. However, given the constraint that the minimum size of the subset is 226, if the number of elements in the initial set is not much bigger than 226 due to limited total number of measurements, we have to allow overlap between subsets which leads to non-negligible similarity between the models learned from different subsets of pairs. Fortunately, even if the similarity is large, this technique will still improve the accuracy of the effective Hamiltonian

computed. Since the predicted model is essentially an interpolation of the effective Hamiltonians that satisfy each pair in the initial set, the predicted energies will not be more noisy than the measured energies due to the nature of interpolation. Therefore, it at least reduces the standard deviation of the distribution of the noise.

B. Double Robust Optimization Plus Rejection

With a real quantum device, the noise in observations and thus in the computed effective Hamiltonian is inevitable, which hinders the classical optimizer from finding the true gate parameters t_j that minimize the state energy. However, we can use robust optimization to mitigate the impact of this noise. Robust optimization is a widely-applied approach to deal with data uncertainty in optimization that does not require the knowledge on the true probability distribution of uncertain data [92, 93]. Robust optimization seeks to find solutions that perform well across a range of possible conditions, rather than optimizing for a specific set of conditions.

Assume some of the $(t_j, E_{measured})$ pairs in the initial set S_{init} are extremely noisy and a fit involving these corrupted pairs will give a bad effective Hamiltonian. We'd like to screen out the pairs that are especially noisy but this is difficult to do in advance. One way to mitigate their impact is to create subsets of S_{init} , in each of which a random portion of pairs in S_{init} are dropped out. Some of these subsets are less likely to have the particularly bad pairs, so if we fit an effective Hamiltonian \tilde{H} from each subset, some of the \tilde{H} 's may be less noisy due to the absence of (at least some of) the bad pairs. Then instead of using the energy calculated using Eq. 6 with one \tilde{H} as loss function for gate parameters optimization, we instead find the gate parameter t_j such that

$$\max\{t_j^\dagger \tilde{H}_k t_j : k = 1, 2, \dots, n_{subset}\} \quad (14)$$

is minimized where n_{subset} is the number of effective Hamiltonians obtained. This is called a worst-case robust optimization of gate parameters.

Finding the gate parameters that minimizes the energy evaluated with different effective Hamiltonians can reduce the impact of a small portion of extremely noisy pairs in the initial set. However, this strategy fails when there is a particularly bad effective Hamiltonian within the collection of all \tilde{H} 's that always gives the worst energy and forces the classical optimizer to accommodate to it. In this case, the gate parameters after optimization may have the state energy calculated with bad \tilde{H} minimized while giving a noiseless state energy worse than before the optimization step. To further reduce the impact of noisy \tilde{H} in the collection of all \tilde{H} 's, we add a second layer of robust optimization: after obtaining a collection of \tilde{H} 's (denoted as $S_{\tilde{H}}$) from all subsets of pairs, we create sub-collections of \tilde{H} 's, in each of which a random portion of \tilde{H} 's in $S_{\tilde{H}}$ are dropped

out. We use each sub-collection to perform worst-case robust optimizations independently, each of which yields a t_j . To select the one that gives the best noiseless energy we do additional quantum measurements for each t_j and the original pre-optimized t_j with more shots per circuit than the shots used for obtaining the observations in S_{init} (see Appendix F). Based on newly measured energies, we choose the best t_j (or reject the optimization move if the original parameters are lowest in energy leaving the gate parameters unchanged).

Algorithm 1 DROPR

Input: Pre-optimized quantum circuit $|\Psi\rangle$, initial set of n_{obs} pairs of $(t_j, E_{measured})$, number of shots per circuit n_{shots} , the index of gate to be optimized j , DROPR parameters n_{subset} , L_{subset} , n_{subcol} , L_{subcol} , n_{dup}
Output: Optimal parameters t_j
 Randomly form n_{subset} overlapping subsets of pairs from the initial set. Each subset has L_{subset} pairs.
for $i = 0$ to $n_{subset} - 1$ **do**
 Convert t_j of each pair in this subset to its quadratic form through Eq. 9 and Eq. 10
 Compute \tilde{H} through linear least square regression using Eq. 8
end for
 Randomly form n_{subcol} overlapping sub-collections of \tilde{H} from the collection of all \tilde{H} obtained. Each sub-collection has L_{subcol} elements.
for $i = 0$ to $n_{subcol} - 1$ **do**
 Find a contender t_j that minimizes Eq. 14
 Measure the energy of the state with the j th gate replaced by a two-qubit unitary generated with contender t_j with $n_{dup} \times n_{shots}$ shots per circuit
end for
 Measure the energy of state $|\Psi\rangle$ with $n_{dup} \times n_{shots}$ shots per circuit
 Select the optimal t_j with the best measured energy (or reject the change if the original state energy is optimal)

The full description of the scheme is shown in Algorithm. 1. This strategy bears resemblance to cross-validation and Metropolis-Hastings Algorithm in Monte Carlo methods and is effective in preventing the algorithm from accepting gate parameters which give plausible state energy calculated with noisy effective Hamiltonian but has noiseless state energy worse than before the optimization step.

Again, in the ideal scheme there shouldn't be overlap between subsets of pairs for effective Hamiltonian fitting. However, given the constraint of minimum size of the subset of pairs being 226, if the size of initial set is small, we have to allow overlap between subsets.

C. GPR and DROPR combined

For the rest of the paper, we will refer to the E-UBOS method with GPR technique as **Eg-UBOS** and the E-UBOS method with DROPR technique as **Ed-UBOS**. Since the GPR technique focuses on expanding the mea-

sured dataset to be more comprehensive for the effective Hamiltonian computation and the DROP technique aims to improve the search for optimal gate parameters given some set of noisy data, we can apply these two techniques in a combined way to take their complementary advantages. The E-UBOS method with both techniques applied is called *Edg-UBOS*.

IV. NUMERICAL COMPARISONS OF APPROACHES

A. Comparing Edg-UBOS with D-UBOS

In this paper, we use the one-dimensional quantum Heisenberg Hamiltonian with open boundary conditions

$$\hat{H} = -h \sum_{j=0}^{n_q} \sigma_j^z - J_z \sum_{j=0}^{n_q-1} \sigma_j^z \sigma_{j+1}^z - J_x \sum_{j=0}^{n_q-1} \sigma_j^x \sigma_{j+1}^x - J_y \sum_{j=0}^{n_q-1} \sigma_j^y \sigma_{j+1}^y \quad (15)$$

for demonstration where n_q is the number of qubits and $J_x = J_y = J_z = h = 1$.

To better understand the performance of UBOS with noisy expectation value measurement, we implement the relevant circuits for UBOS in Qiskit [94] and perform simulations (without hardware noise) on a 4-site 2-layer ansatz and 8-site 4-layer ansatz. To maintain the unitarity of the two-qubit gates in optimization, the ansatz's two-qubit unitary blocks are parameterized with the KAK decomposition [95]. Each gate in our initial circuit is generated randomly by selecting the KAK parameters uniformly at random from $[0, \pi)$.

To avoid ambiguity, for the rest of the paper we will use superscripts to distinguish between the number of shots per circuit for D-UBOS and for methods based on E-UBOS. For example, n_{shots}^D for D-UBOS and n_{shots}^{Edg} for Edg-UBOS.

To study the difference in optimization step quality between Edg-UBOS and D-UBOS given large shot noise, we choose the final state of a D-UBOS run after 10 epochs with 10 shots per circuit whose energy is about 60% off from the optimal VQE energy (for the system size studied, the noiseless state energy plateaus before the 4th epoch). We apply one D-UBOS step with $n_{shots}^D = 20$ on the first gate. Since the result of this application is stochastic, we look at the distribution of the relative energy change, $(E - E_{old})/|E_{old}|$, over a 100 different executions of a D-UBOS step. Then we repeat this procedure using Edg-UBOS steps with $n_{obs} = 450$ and $n_{shots}^{Edg} = 10$ which has roughly the same total number of measurements. As shown in Fig. 1a, we find that two distributions have roughly the same standard deviation, but the distribution for Edg-UBOS has a more negative mean value than that of D-UBOS, which indicates that one

Edg-UBOS step improves the state energy more than one D-UBOS step on average. By comparing the amount of samples with positive relative change in energy, we also notice that Edg-UBOS is much less likely to find “false positive” gate parameters whose noiseless state energy is worse than before optimization. See Appendix D for a detailed discussion on false positive gate parameters.

We also compare the final state energies at which Edg-UBOS and D-UBOS plateau after 10 epochs given large shot noise. As shown in Fig. 1b, the relative energy difference between final states of the D-UBOS and Edg-UBOS runs decays approximately algebraically as

$$(E - E_{old})/|E_{old}| \sim A \times 10^{-\beta N_{meas}} + C$$

where A and C are different constants for each UBOS types and system sizes, and $\beta \sim 2e-7$ ($2e-8$) for ansatz of 4 qubits and depth 2 (8 qubits and depth 4). For the choice of measurement hyperparameters, we start with a set of n_{shots}^D and choose the combination of $(n_{obs}, n_{shots}^{Edg})$ for Edg-UBOS such that the two methods have roughly the same total number of measurements (see Appendix C), prioritizing large n_{obs} . We find that the final state of an Edg-UBOS run has roughly a factor of 3 smaller relative energy error than D-UBOS for all system sizes and total number of measurements studied.

We now consider the plateaued relative energy difference after 10 epochs of various forms of UBOS as we tune the measurement hyperparameters. As shown in Fig. 2(left), the relative energy errors of Edg-UBOS are roughly proportional to $10^{-N_{meas}}$ where the total number of measurements $N_{meas} \propto (n_{obs} \times n_{shots}^{Edg})$ (see Appendix C). For every choice of (n_{obs}, n_{shots}) in Edg-UBOS, we can choose an identical total number of measurements in D-UBOS and again compare the relative error of the energy (see Fig. 2(middle)) and find that for every choice of hyper-parameters, Edg-UBOS is always lower in relative energy error (on average) than D-UBOS (see Fig. 2(right)). The advantage of Edg-UBOS becomes more significant in larger system and when the total number of measurements are less, indicating Edg-UBOS is particularly useful when the noise in quantum measurements is large. See Appendix G for a more detailed discussion of optimal measurement hyperparameter choice.

B. Comparing the effect of each classical technique

To better understand the individual role of our two post-processing approaches, we fix a configuration of the gates and then consider the change in energy induced by the update of a single gate using these approaches. We generate a configuration of the gates by running D-UBOS for 10 epochs using only 10 shots per circuit which reaches an energy of 60% off from the optimal VQE energy. We apply one E-UBOS optimization step (with $n_{obs} = 300$ and $n_{shots}^{Edg} = 10$) with different classical techniques applied (E-UBOS, Edg-UBOS, Ed-UBOS,

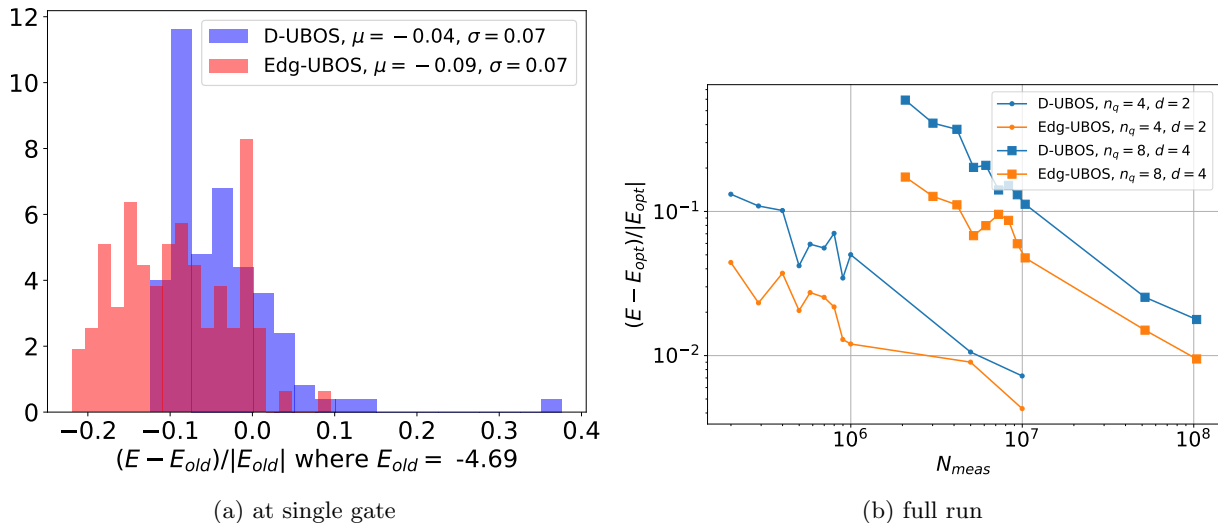


FIG. 1: Histograms of the relative energy change from 100 steps of D-UBOS (blue) with 20 shots per circuit and Edg-UBOS (red) with 450 observations and 10 shots per circuit at the same single gate of an 8-qubit depth-4 ansatz. This corresponds to the same total number of quantum measurements for D-UBOS and Edg-UBOS. (b) Relative energy difference between 10 epochs of UBOS types (different colors) on different system sizes (types of points) and the optimal VQE energy versus number of shots per circuit. Each point averages over the final energies of 5 independent UBOS runs with different random initial states.

Edg-UBOS) on the first gate, and look at the distribution of post-optimization state energy over 100 different executions for each technique. First (see Fig. 3a), we use the same fixed set of 300 observations of $(t_j, E_{measured})$ for all four approaches so that the 100 different executions of each approach differ due to the randomness intrinsic to each classical technique. All techniques improve the energy more often than making it worse. Moreover, all techniques and for essentially all random choices are much better than the E-UBOS step itself motivating the use of these techniques.

The improvement of the energy in the Eg-UBOS step (with GPR technique) can often be large but there is a sizeable probability of making the energy worse than the initial starting energy. The Ed-UBOS step (with DROPR technique) tests the gate parameters it's going to use with additional quantum measurements and reject the change if the energy appears to be getting worse. This means that only a small fraction of the time does the energy get worse and is responsible for the mode in the histogram at the original energy. The rest of the time the energy improves non-trivially but not as much as Eg-UBOS. The Edg-UBOS step (with both techniques) makes a good balance between the effects of both techniques. It not only makes non-trivial improvement to energy but also has strong ability to reject false-positive gate parameters after optimization.

We further test these conclusions on the same gate (and respective configurations) by initializing 100 different initial sets of 300 observations and executing steps of {E-UBOS, Eg-UBOS, Ed-UBOS, Edg-UBOS} independently on each of the initial sets. As shown in Fig. 3b,

Eg-UBOS seems to cause more false-positive cases while having a larger chance to improve energy. Ed-UBOS detects some false-positive cases and rejects the change otherwise mainly improving the energy. Edg-UBOS (with both techniques) takes the complementary advantages of both. We also notice that the distribution of state energy after an E-UBOS step has less negative mean value than the pre-optimization energy, which indicates that an E-UBOS step worsens the energy on average. We attribute this to the fact that the minimum number of pairs is 226 and 300 pairs cannot overconstrain the system enough to reduce the noise in the calculated \hat{H} , which again shows the benefit of these classical post-processing techniques.

As discussed in the previous section, we think that the occurrence of false-positive cases can be greatly reduce if the number of observations is large enough to allow non-overlapping subsets of pairs being assembled in each classical techniques.

V. DISCUSSION AND OUTLOOK

In this paper, we propose Edg-UBOS, a variant of the Unitary Block Optimization Scheme (UBOS) that is well suited for the optimization of quantum circuits on hybrid variational algorithms such as VQE. Edg-UBOS iteratively sweeps over gates. At each step, it calculates an effective Hamiltonian \hat{H} from a system of linear equations obtained from a set of $(t_j, E_{measured})$ observations and then classically finds the gate parameters that minimize the energy with respect to this effective Hamiltonian while keeping the other gates temporarily fixed. Edg-

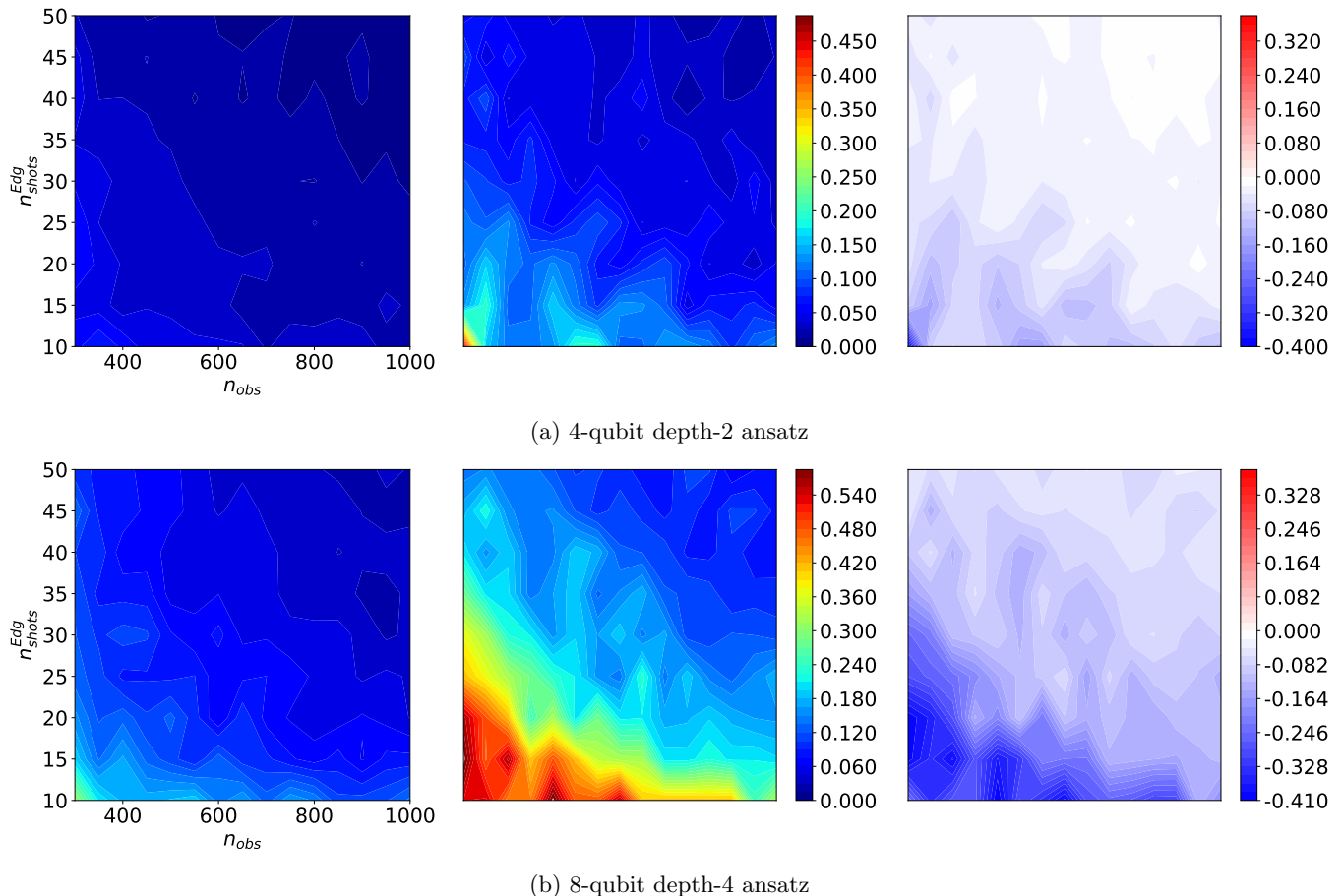


FIG. 2: Filled contour plots of relative energy difference for (a) $n_q = 4$ and $n_d = 2$ and (b) $n_q = 8$ and $n_d = 4$ of Edg-UBOS (left panels), D-UBOS (middle panels), and their difference (right panels) as a function of measurement hyperparameters (n_{shots}^{Edg} and n_{obs} for Edg-UBOS, and n_{shots}^D for D-UBOS with value chosen to match the total number of measurements of Edg-UBOS at each grid point). Each point averages over the final energies of 3 independent UBOS runs with different random initial states. All points in the right panels are negative, showing that Edg-UBOS reaches an energy closer to the optimal VQE energy than D-UBOS regardless of choice of measurement hyperparameters and system size.

UBOS implements additional classical post-processing techniques to improve the accuracy of the effective Hamiltonian calculation and the minimization of the energy. We introduced and benchmarked two schemes: data augmentation using Gaussian Process Regression and Double Robust Optimization Plus Rejection. Data augmentation only requires the original training data, making it a cost-effective approach to increasing the size and diversity of the set of observations. Meanwhile, the DROPR scheme provides a more efficient way to spend the measurement resources. The two techniques combined improves the performance of the algorithm by decreasing the final optimized error by roughly a factor of 3 largely independent of the total number of measurements made.

Edg-UBOS shares all of the standard advantages of D-UBOS including converging an order-of-magnitude faster than stochastic gradient descent (SGD), tunneling through some local minima, and having decreased sensi-

tivity to barren plateaus [83]. Additionally, Edg-UBOS requires lower depths of quantum circuits and has higher resilience to shot noise.

The total number of measurements can be further reduced by strategies such as grouping operators that can be measured jointly [32–34] or by inference methods such as quantum overlapping tomography [35], quantum shadow tomography [36, 37], and classical shadow [38–42]. One can also implement adaptive number of shots per circuit so that the algorithm increases the number of shots per circuit when the energy seems to plateau, which is similar to adaptive learning rate strategy in classical machine learning.

To reach the promise of VQE we need to minimize the total number of measurements while maximizing the accuracy of the final optimization. The development of Edg-UBOS takes an important step toward this goal and places it as one of the primary techniques for VQE on

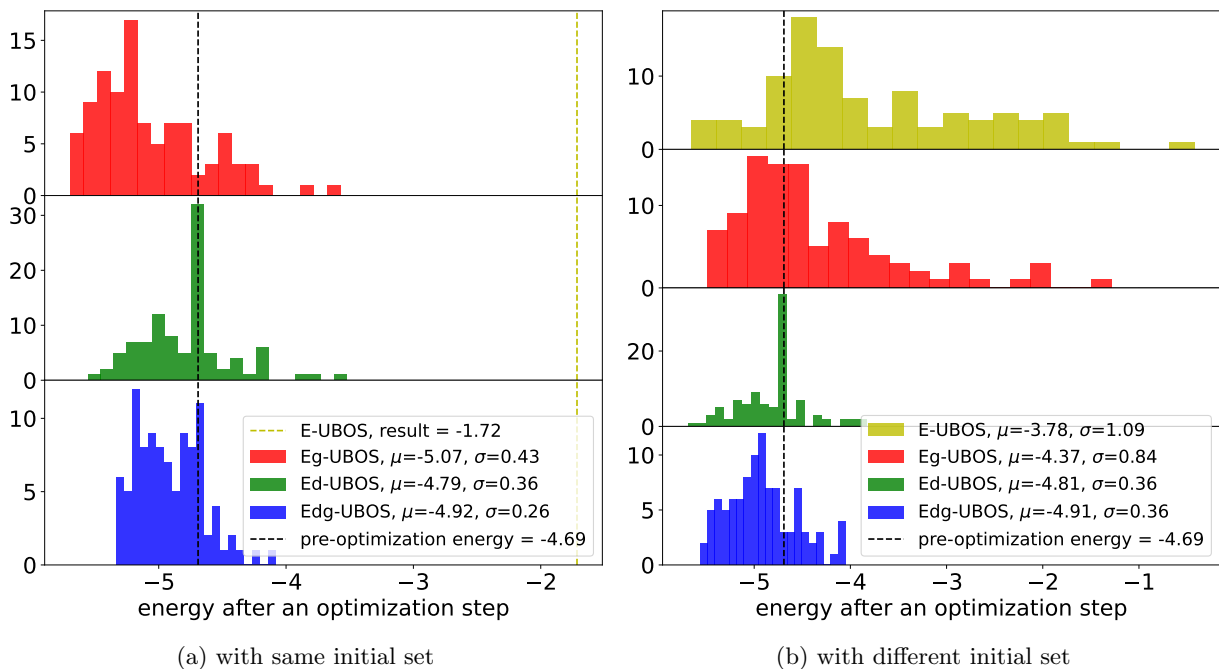


FIG. 3: Histograms of the final energy from 100 optimizations (per approach) of the same single gate of an 8-qubit depth-4 ansatz with 10 shots per circuit. In (a) all trials use the same initial set of 300 pairs of (t_j, E_{noisy}) differing only by the randomness inherent in the techniques. In (b) a new random set of 300 parameters t_j are chosen for each sample.

a quantum computer. Furthermore, it also motivates an important approach toward further improving quantum algorithm through use of non-trivial classical computing resources to make the most effective use of quantum data.

ACKNOWLEDGMENTS

We acknowledge the use of scikit-learn python package [96] and IBM Quantum services [97] for this work.

This work also made use of the Illinois Campus Cluster, a computing resource that is operated by the Illinois Campus Cluster Program (ICCP) in conjunction with the National Center for Supercomputing Applications (NCSA), which is supported by funds from the University of Illinois at Urbana-Champaign.

-
- [1] J. Preskill, *Quantum* **2**, 79 (2018).
 - [2] P. W. Shor, *Proceedings - Annual IEEE Symposium on Foundations of Computer Science, FOCS*, 124 (1994).
 - [3] L. M. Vandersypen, M. Breyta, G. Steffen, C. S. Yannoni, M. H. Sherwood, and I. L. Chuang, *Nature* 2001 414:6866 **414**, 883 (2001).
 - [4] C. Y. Lu, D. E. Browne, T. Yang, and J. W. Pan, *Physical Review Letters* **99**, 250504 (2007).
 - [5] B. P. Lanyon, T. J. Weinhold, N. K. Langford, M. Barbieri, D. F. James, A. Gilchrist, and A. G. White, *Physical Review Letters* **99**, 250505 (2007).
 - [6] E. Lucero, R. Barends, Y. Chen, J. Kelly, M. Mariantoni, A. Megrant, P. O'Malley, D. Sank, A. Vainsencher, J. Wenner, T. White, Y. Yin, A. N. Cleland, and J. M. Martinis, *Nature Physics* 2012 8:10 **8**, 719 (2012).
 - [7] E. Martín-López, A. Laing, T. Lawson, R. Alvarez, X. Q. Zhou, and J. L. O'Brien, *Nature Photonics* 2012 6:11 **6**, 773 (2012).
 - [8] I. L. Markov and M. Saeedi, *Physical Review A - Atomic, Molecular, and Optical Physics* **87**, 012310 (2013).
 - [9] M. Amico, Z. H. Saleem, and M. Kumph, *Physical Review A* **100**, 012305 (2019).
 - [10] L. K. Grover, *Proceedings of the Annual ACM Symposium on Theory of Computing Part F129452*, 212 (1996).
 - [11] C. H. Bennett, E. Bernstein, G. Brassard, and U. Vazirani, <https://doi.org/10.1137/S0097539796300933> **26**, 1510 (2006).
 - [12] N. J. Cerf, L. K. Grover, and C. P. Williams, *Applicable Algebra in Engineering, Communications and Computing* **10**, 311 (2000).
 - [13] A. Ambainis, *SIGACT News* **35**, 22–35 (2004).

- [14] A. Ambainis, *SIAM Journal on Computing* **37**, 210 (2007), <https://doi.org/10.1137/S0097539705447311>.
- [15] D. J. Bernstein, *Lecture Notes in Computer Science (including subseries Lecture Notes in Artificial Intelligence and Lecture Notes in Bioinformatics)* **6061 LNCS**, 73 (2010).
- [16] M. Suchara, Y. Alexeev, F. Chong, H. Finkel, H. Hoffmann, J. Larson, J. Osborn, and G. Smith, *Proceedings of the 3rd International Workshop on Post-Moore's Era Supercomputing*, 3 (2014).
- [17] A. Peruzzo, J. McClean, P. Shadbolt, M. H. Yung, X. Q. Zhou, P. J. Love, A. Aspuru-Guzik, and J. L. O'Brien, *Nature Communications* 2014 5:1 **5**, 1 (2014).
- [18] A. Khamoshi, G. P. Chen, F. A. Evangelista, al, J. S. Kottmann, S. Alperin-Lea, T. Tamayo-Mendoza, J. R. McClean, J. Romero, R. Babbush, and A. Aspuru-Guzik, *New Journal of Physics* **18**, 023023 (2016).
- [19] J. Tilly, H. Chen, S. Cao, D. Picozzi, K. Setia, Y. Li, E. Grant, L. Wossnig, I. Rungger, G. H. Booth, and J. Tennyson, *Physics Reports* **986**, 1 (2021).
- [20] P. Deglmann, A. Schäfer, and C. Lennartz, *International Journal of Quantum Chemistry* **115**, 107 (2015).
- [21] B. J. Williams-Noonan, E. Yuriev, and D. K. Chalmers, *Journal of Medicinal Chemistry* **61**, 638 (2018).
- [22] M. A. Continentino, *Key Methods and Concepts in Condensed Matter Physics* (2021), 10.1088/978-0-7503-3395-5.
- [23] A. V. D. Ven, Z. Deng, S. Banerjee, and S. P. Ong, *Chemical Reviews* **120**, 6977 (2020).
- [24] M. A. Nielsen and I. L. Chuang, *Quantum Computation and Quantum Information* (2010), 10.1017/CBO9780511976667.
- [25] A. Kandala, A. Mezzacapo, K. Temme, M. Takita, M. Brink, J. M. Chow, and J. M. Gambetta, *Nature* 2017 549:7671 **549**, 242 (2017).
- [26] J. Tilly, P. V. Sriluckshmy, A. Patel, E. Fontana, I. Rungger, E. Grant, R. Anderson, J. Tennyson, and G. H. Booth, *Physical Review Research* **3** (2021), 10.1103/PhysRevResearch.3.033230.
- [27] D. Wecker, M. B. Hastings, and M. Troyer, *Physical Review A* **92**, 042303 (2015).
- [28] J. Romero, R. Babbush, J. R. McClean, C. Hempel, P. J. Love, and A. Aspuru-Guzik, *Quantum Science and Technology* **4**, 014008 (2018).
- [29] P. K. Barkoutsos, J. F. Gonthier, I. Sokolov, N. Moll, G. Salis, A. Fuhrer, M. Ganzhorn, D. J. Egger, M. Troyer, A. Mezzacapo, S. Filipp, and I. Tavernelli, *Physical Review A* **98**, 022322 (2018).
- [30] B. T. Gard, L. Zhu, G. S. Barron, N. J. Mayhall, S. E. Economou, and E. Barnes, *npj Quantum Information* 2020 6:1 **6**, 1 (2020).
- [31] H. R. Grimsley, S. E. Economou, E. Barnes, and N. J. Mayhall, *Nature Communications* 2019 10:1 **10**, 1 (2019).
- [32] P. Gokhale, O. Angiuli, Y. Ding, K. Gui, T. Tomesh, M. Suchara, M. Martonosi, and F. T. Chong, "Minimizing state preparations in variational quantum eigensolver by partitioning into commuting families," (2019).
- [33] I. Hamamura and T. Imamichi, *npj Quantum Information* 2020 6:1 **6**, 1 (2020).
- [34] W. J. Huggins, J. R. McClean, N. C. Rubin, Z. Jiang, N. Wiebe, K. B. Whaley, and R. Babbush, *npj Quantum Information* 2021 7:1 **7**, 1 (2021).
- [35] J. Cotler and F. Wilczek, *Physical Review Letters* **124**, 100401 (2020).
- [36] S. Aaronson, "Shadow tomography of quantum states," (2018), arXiv:1711.01053 [quant-ph].
- [37] S. Aaronson and G. N. Rothblum, *Proceedings of the Annual ACM Symposium on Theory of Computing*, 322 (2019).
- [38] H. Y. Huang, R. Kueng, and J. Preskill, *Nature Physics* 2020 16:10 **16**, 1050 (2020).
- [39] T. E. O'Brien, M. Streif, N. C. Rubin, R. Santagati, Y. Su, W. J. Huggins, J. J. Goings, N. Moll, E. Kyoseva, M. Degroote, C. S. Tautermann, J. Lee, D. W. Berry, N. Wiebe, and R. Babbush, *Physical Review Research* **4** (2021), 10.1103/PhysRevResearch.4.043210.
- [40] C. Hadfield, S. Bravyi, R. Raymond, and A. Mezzacapo, *Communications in Mathematical Physics* **391**, 951 (2020).
- [41] C. Hadfield, "Adaptive pauli shadows for energy estimation," (2021).
- [42] J. M. Lukens, K. J. Law, and R. S. Bennink, *npj Quantum Information* 2021 7:1 **7**, 1 (2021).
- [43] Y. Li and S. C. Benjamin, *Physical Review X* **7**, 021050 (2017).
- [44] K. Temme, S. Bravyi, and J. M. Gambetta, *Physical Review Letters* **119**, 180509 (2017).
- [45] T. Giurgica-Tiron, Y. Hindy, R. Larose, A. Mari, and W. J. Zeng, *Proceedings - IEEE International Conference on Quantum Computing and Engineering, QCE 2020*, 306 (2020).
- [46] M. Krebsbach, B. Trauzettel, and A. Calzona, *Physical Review A* **106**, 062436 (2022).
- [47] Y. Kim, C. J. Wood, T. J. Yoder, S. T. Merkel, J. M. Gambetta, K. Temme, and A. Kandala, *Nature Physics* 2023 19:5 **19**, 752 (2023).
- [48] S. Endo, S. C. Benjamin, and Y. Li, *Physical Review X* **8**, 031027 (2018).
- [49] A. He, B. Nachman, W. A. D. Jong, and C. W. Bauer, *Physical Review A* **102**, 012426 (2020).
- [50] Y. Kim, A. Eddins, S. Anand, K. X. Wei, E. van den Berg, S. Rosenblatt, H. Nayfeh, Y. Wu, M. Zaletel, K. Temme, and A. Kandala, *Nature* 2023 618:7965 **618**, 500 (2023).
- [51] E. van den Berg, Z. K. Mineev, A. Kandala, and K. Temme, *Nature Physics* 2023 19:8 **19**, 1116 (2023).
- [52] S. Ferracin, A. Hashim, J.-L. Ville, R. Naik, A. Carignan-Dugas, H. Qassim, A. Morvan, D. I. Santiago, I. Siddiqi, and J. J. Wallman, "Efficiently improving the performance of noisy quantum computers," (2022), arXiv:2201.10672 [quant-ph].
- [53] C. Piveteau, D. Sutter, and S. Woerner, *npj Quantum Information* 2022 8:1 **8**, 1 (2022).
- [54] S. Chen, W. Yu, P. Zeng, and S. T. Flammia, *PRX Quantum* **2**, 030348 (2021).
- [55] A. Strikis, D. Qin, Y. Chen, S. C. Benjamin, and Y. Li, *PRX Quantum* **2**, 040330 (2021).
- [56] P. Czarnik, A. Arrasmith, P. J. Coles, and L. Cincio, *Quantum* **5**, 592 (2021).
- [57] C. G. Broyden, *IMA Journal of Applied Mathematics* **6**, 76 (1970).
- [58] F. R., *The Computer Journal* **13**, 317 (1970).
- [59] D. Goldfarb, *Mathematics of Computation* **24**, 23 (1970).
- [60] D. F. Shanno, *Mathematics of Computation* **24**, 647 (1970).
- [61] S. I. Amari, *Neural Computation* **10**, 251 (1998).

- [62] J. Martens and D. London, *Journal of Machine Learning Research* **21**, 1 (2014).
- [63] D. Wierichs, C. Gogolin, and M. Kastoryano, *Physical Review Research* **2**, 043246 (2020).
- [64] W. Lavrijsen, A. Tudor, J. Muller, C. Iancu, and W. D. Jong, *Proceedings - IEEE International Conference on Quantum Computing and Engineering, QCE 2020*, 267 (2020).
- [65] A. Pellow-Jarman, I. Sinayskiy, A. Pillay, and F. Petruccione, *Quantum Information Processing* **20**, 1 (2021).
- [66] R. M. Parrish, J. T. Iosue, A. Ozaeta, and P. L. McMahon, “A jacobi diagonalization and anderson acceleration algorithm for variational quantum algorithm parameter optimization,” (2019).
- [67] K. M. Nakanishi, K. Fujii, and S. Todo, *Physical Review Research* **2**, 043158 (2020).
- [68] D. Luo, J. Shen, R. Dangovski, and M. Soljačić, “Quack: Accelerating gradient-based quantum optimization with koopman operator learning,” (2023), arXiv:2211.01365 [quant-ph].
- [69] S. Wang, S. Sankaran, H. Wang, and P. Perdikaris, “An expert’s guide to training physics-informed neural networks,” (2023), arXiv:2308.08468 [cs.LG].
- [70] M. Benedetti, E. Lloyd, S. Sack, and M. Fiorentini, *Quantum Science and Technology* **4**, 043001 (2019).
- [71] J. G. Liu and L. Wang, *Physical Review A* **98**, 062324 (2018).
- [72] C. Hempel, C. Maier, J. Romero, J. McClean, T. Monz, H. Shen, P. Jurcevic, B. P. Lanyon, P. Love, R. Babush, A. Aspuru-Guzik, R. Blatt, and C. F. Roos, *Physical Review X* **8**, 031022 (2018).
- [73] R. Sagastizabal, X. Bonet-Monroig, M. Singh, M. A. Rol, C. C. Bultink, X. Fu, C. H. Price, V. P. Ostroukh, N. Muthusubramanian, A. Bruno, M. Beekman, N. Haider, T. E. O’Brien, and L. Dicarlo, *Physical Review A* **100**, 010302 (2019).
- [74] J. M. Kübler, A. Arrasmith, L. Cincio, and P. J. Coles, *Quantum* **4**, 263 (2020).
- [75] K. Mitarai, M. Negoro, M. Kitagawa, and K. Fujii, *Physical Review A* **98**, 032309 (2018).
- [76] G. Nannicini, *Physical Review E* **99**, 013304 (2019).
- [77] D. Wang, O. Higgott, and S. Brierley, *Physical Review Letters* **122**, 140504 (2019).
- [78] R. M. Parrish, E. G. Hohenstein, P. L. McMahon, and T. J. Martínez, *Physical Review Letters* **122**, 230401 (2019).
- [79] M. Foss-Feig, D. Hayes, J. M. Dreiling, C. Figgatt, J. P. Gaebler, S. A. Moses, J. M. Pino, and A. C. Potter, *Physical Review Research* **3** (2020), 10.1103/PhysRevResearch.3.033002.
- [80] K. M. Nakanishi, K. Mitarai, and K. Fujii, *Physical Review Research* **1**, 033062 (2019).
- [81] W. J. Huggins, J. Lee, U. Baek, B. O’Gorman, and K. B. Whaley, *New Journal of Physics* **22**, 073009 (2020).
- [82] I. G. Ryabinkin, S. N. Genin, and A. F. Izmaylov, *Journal of Chemical Theory and Computation* **15**, 249 (2019).
- [83] L. Slattery, B. Villalonga, and B. K. Clark, *Phys. Rev. Res.* **4**, 023072 (2022).
- [84] S. Wang, E. Fontana, M. Cerezo, K. Sharma, A. Sone, L. Cincio, and P. J. Coles, *Nature Communications* 2021 12:1 **12**, 1 (2021).
- [85] A. Pérez-Salinas, H. Wang, and X. Bonet-Monroig, *npj Quantum Information* 2024 10:1 **10**, 1 (2024).
- [86] G. Buonaiuto, F. Gargiulo, G. D. Pietro, M. Esposito, and M. Pota, *Quantum Machine Intelligence* 2024 6:1 **6**, 1 (2024).
- [87] H. Zhang, M. Cisse, Y. N. Dauphin, and D. Lopez-Paz, “mixup: Beyond empirical risk minimization,” (2018), arXiv:1710.09412 [cs.LG].
- [88] H. Mei, T. Zhao, S. Tang, H. Qiu, L. Wang, M. Zhang, F. Meng, and H. Li, “Grstdet: Learning to generate local reverse samples for few-shot object detection,” (2023), arXiv:2312.16571 [cs.CV].
- [89] Y. Zhao, J. Tourais, I. Pierce, C. Nitsche, T. A. Treibel, S. Weingärtner, A. M. Schweidtmann, and Q. Tao, “Bayesian uncertainty estimation by hamiltonian monte carlo: Applications to cardiac mri segmentation,” (2024), arXiv:2403.02311 [eess.IV].
- [90] J. Wang, *Computing in Science and Engineering* **25**, 4–11 (2023).
- [91] Y. Shi, *The Gradient* (2019).
- [92] B. L. Gorissen, I. Yanikoglu, and D. den Hertog, *Omega* **53**, 124–137 (2015).
- [93] A. Ben-Tal, L. Ghaoui, and A. Nemirovski, *Robust Optimization*, Princeton Series in Applied Mathematics (Princeton University Press, 2009).
- [94] Qiskit contributors, “Qiskit: An open-source framework for quantum computing,” (2023).
- [95] R. R. Tucci, “An introduction to cartan’s kak decomposition for qc programmers,” (2005), arXiv:quant-ph/0507171 [quant-ph].
- [96] F. Pedregosa, G. Varoquaux, A. Gramfort, V. Michel, B. Thirion, O. Grisel, M. Blondel, P. Prettenhofer, R. Weiss, V. Dubourg, J. Vanderplas, A. Passos, D. Cournapeau, M. Brucher, M. Perrot, and E. Duchesnay, *Journal of Machine Learning Research* **12**, 2825 (2011).
- [97] IBM Quantum, (2021).
- [98] D. M. Goerz, “Decomposing two-qubit hamiltonians into pauli-matrices,” (2014).
- [99] I. A. Luchnikov, M. E. Krechetov, and S. N. Filippov, *New Journal of Physics* **23**, 073006 (2021).
- [100] T. Abrudan, J. Eriksson, and V. Koivunen, in *2008 IEEE International Conference on Acoustics, Speech and Signal Processing* (2008) pp. 2353–2356.

Appendix A: Parameterize the gate using KAK decomposition

In UBOS algorithms, we parameterize the generic two-qubit unitaries by two-qubit Pauli operators [98]. However, to ensure that the gate remains unitary after optimization, we also parameterize the two-qubit gate using the Cartan (KAK) decomposition for $U \in SU(4)$ [95] as

$$U = (A_0 \otimes A_1)(e^{-i\vec{k}\cdot\vec{\Sigma}})(B_0 \otimes B_1) \quad (\text{A.1})$$

where $\vec{k} \in \mathbb{R}^3$, $\vec{\Sigma} = (P^{XX}, P^{YY}, P^{ZZ})$, and A_0, A_1, B_0 , and $B_1 \in SU(2)$ are generic one-qubit $U3$ gates parameterized by three real parameters as

$$U3(\theta, \lambda, \phi) = \begin{bmatrix} \cos(\theta/2) & -e^{i\lambda}\sin(\theta/2) \\ e^{i\phi}\sin(\theta/2) & e^{i(\lambda+\phi)}\cos(\theta/2) \end{bmatrix} \quad (\text{A.2})$$

The two-qubit gate U resulting from Eq. A.1 is therefore parameterized with 15 real parameters (denoted as θ_j) and is unitary regardless of choice of θ_j . Since the KAK decomposition we use does not have the global phase term, we cannot deterministically convert the gate parameterization from t_j form to θ_j form. However, the conversion from θ_j form to t_j form is deterministic since the coefficients of Pauli decomposition is unique. Therefore, to ensure the unitarity of the gate after optimization, the two-qubit unitaries of the ansatz is stored in t_j form and is only converted to θ_j form before being fed to classical optimizer.

To avoid this redundancy of using θ_j , a possible approach is to perform gradient descent on a Riemannian manifold of unitary matrices [99, 100].

Appendix B: Measurement circuit for different types of UBOS

The energy of a quantum state can be found as $E = \sum_i \text{Tr}(\rho_i \hat{h}_i)$ where \hat{h}_i are the components of the Hamiltonian and ρ is the reduced density matrix of the state. In E-UBOS, we obtain the state energy by measuring all Hamiltonian components with circuit shown in Fig. A1 and perform linear combination as the following:

$$\begin{aligned} \text{Tr}(\rho \hat{Z}) &= P(0) - P(1) \\ \text{Tr}(\rho \widehat{XX}) &= 2P(+, +) + 2P(-, -) - 1 \\ \text{Tr}(\rho \widehat{YY}) &= 2P(+i, +i) + 2P(-i, -i) - 1 \\ \text{Tr}(\rho \widehat{ZZ}) &= P(0, 0) - P(0, 1) - P(1, 0) + P(1, 1) \end{aligned} \quad (\text{B.1})$$

where $P(\cdot)$ is the probability of measuring corresponding states.

The Hadamard test circuit for \tilde{H} matrix element measurement in D-UBOS is shown in Fig. A2.

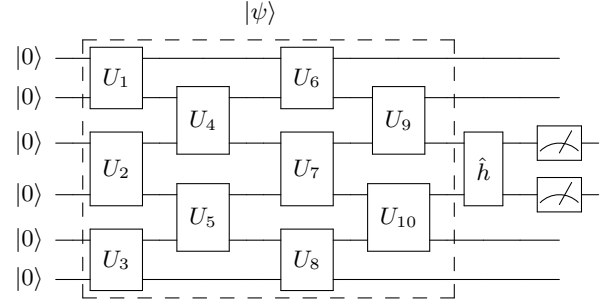


FIG. A1: Quantum circuit for E-UBOS measurement. The circuit shown is an example of measuring expectation value of a two-qubit operator acting on the 3rd and 4th qubit using a 6-qubit depth-4 ansatz.

Appendix C: Calculating total number of measurements

The total number of measurements is defined as

$$N_{meas} = N_{step} \times N_{element} \times N_{operator} \times n_{shots} \quad (\text{C.1})$$

where $N_{step} = N_{epoch} \times N_{gate}$ is the number of optimization steps, the number of gates in the ansatz N_{gate} is a constant determined by the number of qubit n_q and the circuit depth d , the number of training epochs N_{epoch} is a algorithm hyperparameter, $N_{element}$ is the number of matrix elements or observations to obtain the effective Hamiltonian, and $N_{operator}$ is the number of unique operators in the Hamiltonian.

The Hamiltonian studied contains only local $\{Z, XX, YY, ZZ\}$ operators. For an ansatz of n_q qubits, we need to measure n_q unique Z operators acting on different qubits. For the three kinds of two-qubit operators, due to the open boundary condition of the ansatz, there exists $(n_q - 1)$ unique operators of each kind. Therefore, the total number of unique operators in the Hamiltonian is $4n_q - 3$.

The total number of measurements for D-UBOS and Edg-UBOS are calculated as

$$N_{meas}^D = N_{step} \times 256 \times (4n_q - 3) \times n_{shots}^D \quad (\text{C.2})$$

$$N_{meas}^{Edg} = N_{step} \times (n_{obs} + 60) \times (4n_q - 3) \times n_{shots}^{Edg} \quad (\text{C.3})$$

where 256 is the unique real parameters of the effective Hamiltonian, and 60 is the empirically-chosen number of additional observations for testing the contender gate parameters in DROPR scheme.

Appendix D: How noise makes the optimization plateau

To understand how noisy measurement outcomes lead to energy plateauing above the optimal energy, we consider the change in noisy state energy and in noiseless

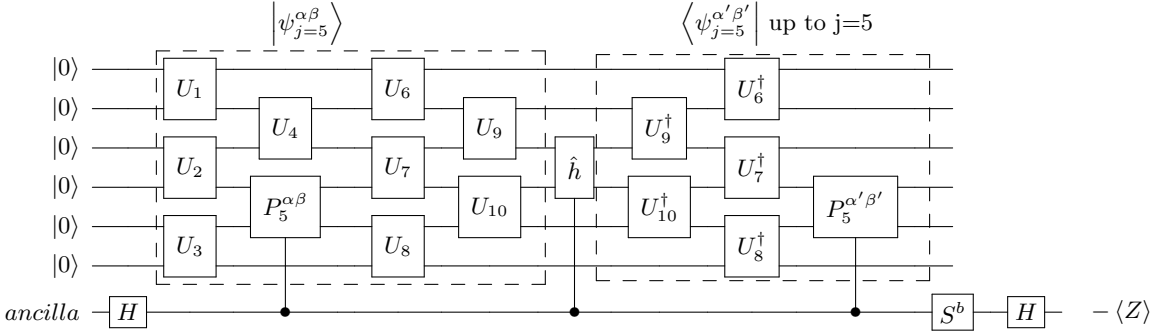


FIG. A2: Quantum circuit for measuring \tilde{H} matrix elements in D-UBOS. The circuit shown is an example for measuring $\tilde{H}^{\alpha'\beta';\alpha\beta}$ at $j = 5$ th gate using a 6-qubit, depth-4 ansatz. The unitary operator \hat{h} is one of the Hamiltonian components. The $j = 5$ th gate of $|\psi_{j=5}^{\alpha\beta}\rangle$, $\langle\psi_{j=5}^{\alpha'\beta'}|$, and \hat{h} are controlled by the ancilla qubit. The adjoint of the gates are applied to the circuit up to $j = 5$ th gate because the rest of the gates will not affect the measurement outcome. When the boolean $b = 0$ ($b = 1$), the real (imaginary) part of the expectation value is estimated by $-\langle Z \rangle$.

state energy after one optimization step. We choose the state of a D-UBOS run after 10 epochs with 10 shots per circuit whose energy is about 60% off from the optimal VQE energy. We apply one D-UBOS step with $n_{shots}^D = 20$ on the same gate of 100 identical state. As shown in Fig. A3a, for a D-UBOS step, the classical optimizer always improves the noisy energy calculated with \tilde{H} , but the noiseless energy gets worse in most cases and is very different from the noisy energy, which we refer to as a "false-positive case". The excessive noise in measured \tilde{H} makes it possible for classical optimizer to find an unphysical noisy state energy below the optimal VQE energy of the ansatz. Then we repeat this procedure using Edg-UBOS steps with $n_{obs} = 450$ and $n_{shots}^{Edg} = 10$ which has roughly the same total number of measurements (see Fig. A3b). We find that even though the improvement in noisy energy by an Edg-UBOS step is much smaller than that by a D-UBOS step, the noiseless energy is improved in most cases, which indicates that Edg-UBOS can effectively suppress the noise in the effective Hamiltonian (due to noisy quantum measurements) and make non-trivial improvements to the noiseless energy. Besides, the noiseless energy after an Edg-UBOS step is much closer to the noisy energy, showing the algorithm's high accuracy in state energy estimation, which is very important for convergence detection towards the end of its run.

Then we execute three independent D-UBOS runs with 20 shots per circuit and three Edg-UBOS runs with 450 observations and 10 shots per circuit on different random initial states. We look at the change in relative energy error throughout the full runs (see Fig. A4). We find that Edg-UBOS always plateau at an energy level much better than D-UBOS. Moreover, even though the relative energy error can get worse after one optimization step due to noise in quantum measurement outcomes, the scale of such setback is much smaller in Edg-UBOS, which is much favorable for variational algorithms.

Appendix E: GPR parameters

The GPR scheme has several hyperparameters including the number and size of subsets, the choice of kernel function, and the number of artificial data generated with each model. In this paper, we empirically choose to make 60 subsets with size equal to 60% of the initial set size. We use the Radial Basis Function (RBF) kernel with length scale of 1 for the Gaussian Process Regressor. The number of artificial data generated per model is 2% of the initial set size.

In principle, one can generate arbitrarily large amount of artificial data at the cost of classical computing resources. To understand the relationship between the amount of artificial data and the effect of the GPR scheme, we fix a configuration of the gates and then consider the change in energy induced by the update of a single gate using Eg-UBOS with different number of artificial data generated per model. Again we choose the state of a D-UBOS run after 10 epochs with 10 shots per circuit whose energy is about 60% off from the optimal VQE energy. We apply one Eg-UBOS optimization step (with $n_{obs} = 450$ and $n_{shots}^{Edg} = 10$) with different number of artificial data generated per model on the first gate, and look at the mean and standard deviation of the distributions of post-optimization state energy over 100 different executions for each hyperparameter choice. As shown in Fig. A5, both the mean and the standard deviation of the distribution don't change much as the number of artificial data generated per model increases. Since the number of subsets is 60, generating 10 artificial pairs per model means 600 artificial pairs which is already larger than the amount of pairs in the initial set which is 450. Therefore, it is unlikely to further increase the diversity and comprehensiveness of the augmented data set by further generation of artificial data, leading to similar mean and standard deviation of the distribution of post-optimization state energy for all choices of

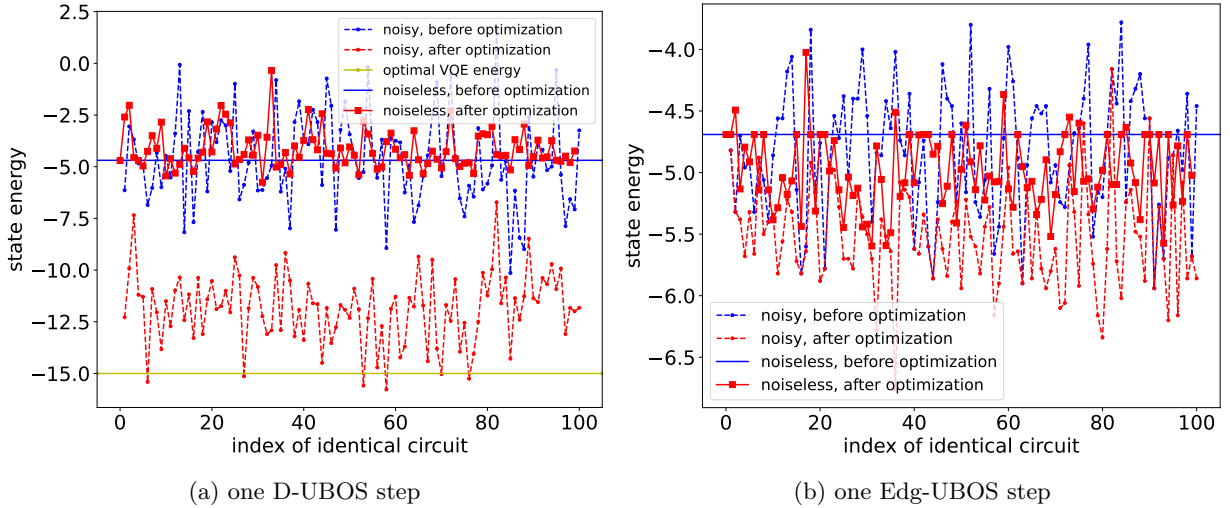


FIG. A3: The change in noisy state energy and noiseless state energy after a D-UBOS (a) and an Edg-UBOS (b) optimization step on the same gate of 100 identical circuits using ansatz of 8-qubit depth-4. The noisy state energy is always improved by the classical optimizer using the noisy \tilde{H} . For D-UBOS, the noiseless energy worsens after optimization on average; for Edg-UBOS, the noiseless energy improves on average (the optimal VQE energy is -15).

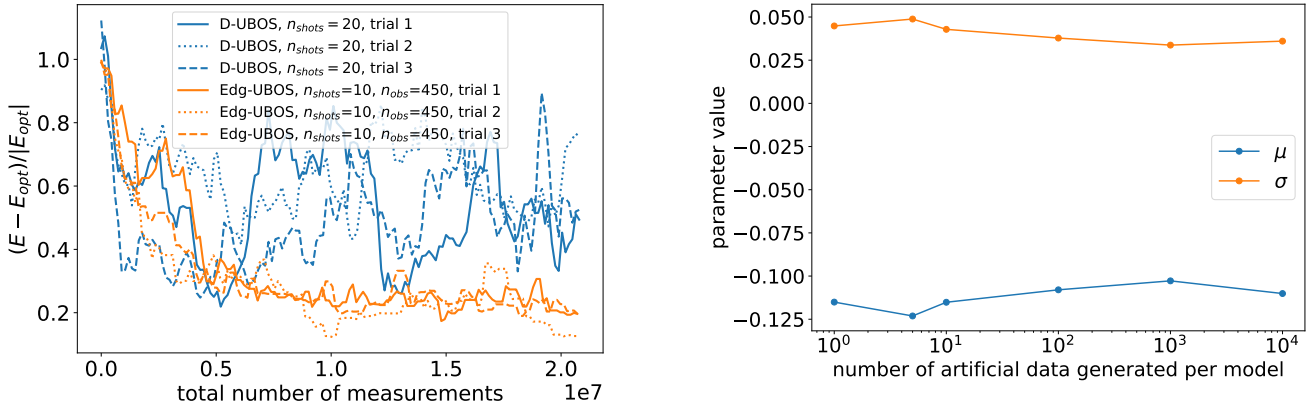


FIG. A4: Relative energy error for $n_q = 8$ and $n_d = 4$ as a function of total number of measurements during three different optimization runs of D-UBOS (blue; 20 shots per circuit) and Edg-UBOS (orange; 10 shots per circuit, 450 observations, which correspond to the same number of measurements per UBOS step).

number of artificial data generated per model.

Appendix F: DROPR energy measurement for contender gate parameters

In the DROPR scheme, we find the energy of the state assembled with each contender gate parameters t_j through additional quantum measurements. Even though we spend more shots per circuit for these measurements, the outcome is still going to be noisy. An alternative approach is to measure the same state sev-

FIG. A5: Mean (blue) and standard deviation (orange) of distributions of post-optimization state energy from 100 different optimization steps on the first gate of identical state as a function of numbers of artificial data generated per Gaussian Process model.

eral times, each with the same shots per circuit as in measuring observations (n_{shots}^{Edg}), and averaging the obtained energies. To spend the measurement resources more efficiently, we compare the accuracy of measured energy obtained by measuring the state one time with $10N$ shots per circuit to measuring the identical state N times with 10 shots per circuit and averaging the measured energies. We choose a random state and measure its energy 100 times independently with each of these two methods, and repeat with different values of N . We look at the mean and standard deviation of the distributions of the energy error (see Fig. A6). We find that, when N is small such that the $(10N)$ -shots measurement outcome is still very noisy, averaging over many noisy measured

energies is slightly more accurate than one less noisy measured energies. Some interesting open questions include that whether this conclusion holds as N further increases and that if there exists a deterministic optimal shots per circuit for each measurement instead of 10 which is empirically chosen.

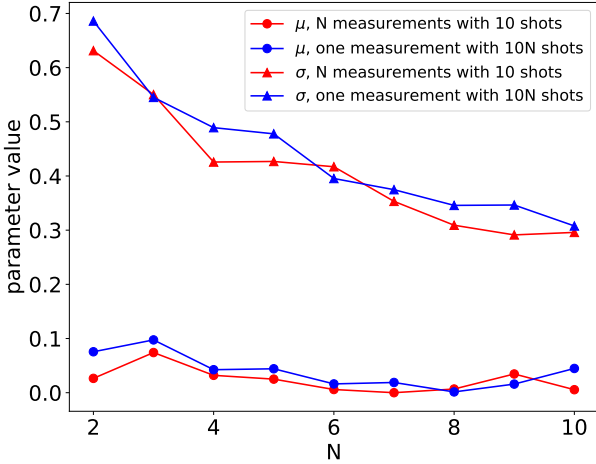


FIG. A6: Mean (circle marker) and standard deviation (triangle marker) of distribution of state energy errors measured one time with $10N$ (blue) shots per circuit and measured N time with 10 shots (red) as a function of N .

Appendix G: Edg-UBOS optimal hyperparameter choice

We consider the optimal choice of measurement hyperparameters for Edg-UBOS, n_{shots}^{Edg} and n_{obs} , given roughly the same total amount of measurement (see Fig. A7). we find that, in the range studied, n_{shots}^{Edg} and n_{obs} have no priority over each other so it's better to increase both hyperparameters following an alternating pattern to minimize the relative energy error to the optimal VQE energy. The difference in relative energy error to the best VQE energy between the optimal choice and the non-optimal choice is less than 5%, which implies some flexibility in hyperparameter tuning.

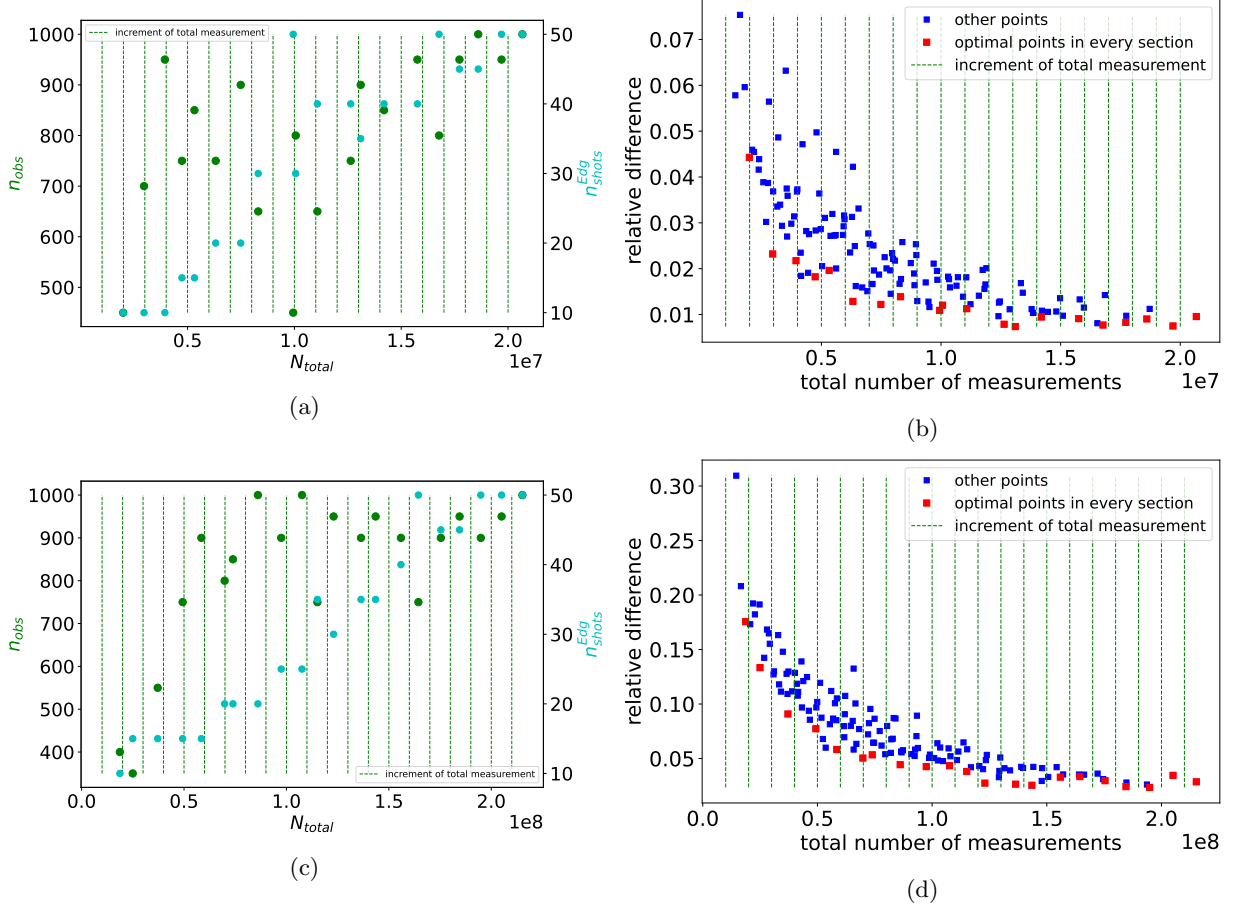


FIG. A7: Optimal choices of measurement hyperparameters (n_{shots} , n_{obs}) for (a-b) a 4-qubit depth-2 ansatz and (c-d) an 8-qubit depth-4 ansatz. The left panels show the optimal choice of hyperparameters for each interval of total number of measurements of each system size. The right panels show their final optimized energy error averaged over the final energies of 3 independent UBOS runs with different random initial states. The optimal combinations of n_{obs} and n_{shots} helps the algorithm reach a few percent closer to the optimal VQE energy than the non-optimal choices.